



FDG PET/CT radiomics as a tool to differentiate between reactive axillary lymphadenopathy following COVID-19 vaccination and metastatic breast cancer axillary lymphadenopathy: a pilot study

Michal Eifer^{1,2} · Hodaya Pinian¹ · Eyal Klang^{1,2,3} · Yousef Alhoubani¹ · Nayroz Kanana^{1,2} · Noam Tau^{1,2} · Tima Davidson^{1,2} · Eli Konen^{1,2} · Onofrio A. Catalano⁴ · Yael Eshet^{1,2} · Liran Domachevsky^{1,2}

Received: 30 January 2022 / Revised: 6 March 2022 / Accepted: 9 March 2022 / Published online: 6 April 2022
© The Author(s), under exclusive licence to European Society of Radiology 2022

Abstract

Objectives To evaluate if radiomics with machine learning can differentiate between F-18-fluorodeoxyglucose (FDG)-avid breast cancer metastatic lymphadenopathy and FDG-avid COVID-19 mRNA vaccine-related axillary lymphadenopathy.

Materials and methods We retrospectively analyzed FDG-positive, pathology-proven, metastatic axillary lymph nodes in 53 breast cancer patients who had PET/CT for follow-up or staging, and FDG-positive axillary lymph nodes in 46 patients who were vaccinated with the COVID-19 mRNA vaccine. Radiomics features (110 features classified into 7 groups) were extracted from all segmented lymph nodes. Analysis was performed on PET, CT, and combined PET/CT inputs. Lymph nodes were randomly assigned to a training ($n = 132$) and validation cohort ($n = 33$) by 5-fold cross-validation. K-nearest neighbors (KNN) and random forest (RF) machine learning models were used. Performance was evaluated using an area under the receiver-operator characteristic curve (AUC-ROC) score.

Results Axillary lymph nodes from breast cancer patients ($n = 85$) and COVID-19-vaccinated individuals ($n = 80$) were analyzed. Analysis of first-order features showed statistically significant differences ($p < 0.05$) in all combined PET/CT features, most PET features, and half of the CT features. The KNN model showed the best performance score for combined PET/CT and PET input with 0.98 (± 0.03) and 0.88 (± 0.07) validation AUC, and 96% ($\pm 4\%$) and 85% ($\pm 9\%$) validation accuracy, respectively. The RF model showed the best result for CT input with 0.96 (± 0.04) validation AUC and 90% ($\pm 6\%$) validation accuracy.

Conclusion Radiomics features can differentiate between FDG-avid breast cancer metastatic and FDG-avid COVID-19 vaccine-related axillary lymphadenopathy. Such a model may have a role in differentiating benign nodes from malignant ones.

Key Points

- Patients who were vaccinated with the COVID-19 mRNA vaccine have shown FDG-avid reactive axillary lymph nodes in PET-CT scans.
- We evaluated if radiomics and machine learning can distinguish between FDG-avid metastatic axillary lymphadenopathy in breast cancer patients and FDG-avid reactive axillary lymph nodes.
- Combined PET and CT radiomics data showed good test AUC (0.98) for distinguishing between metastatic axillary lymphadenopathy and post-COVID-19 vaccine-associated axillary lymphadenopathy. Therefore, the use of radiomics may have a role in differentiating between benign from malignant FDG-avid nodes.

Keywords Machine learning · PET-CT · Lymphadenopathy · COVID-19 vaccine · Breast cancer

✉ Michal Eifer
michaleifer@gmail.com

¹ Department of Diagnostic Imaging, Chaim Sheba Medical Center, 2 Sheba Road, 5266202 Ramat Gan, Israel

² Sackler Faculty of Medicine, Tel Aviv University, Tel Aviv, Israel

³ ARC Center for Digital Innovation, Chaim Sheba Medical Center, Ramat Gan, Israel

⁴ Department of Radiology, Massachusetts General Hospital, Harvard Medical School, Boston, MA, USA

Abbreviations

COVID-19	Coronavirus disease 2019
CV	Cross-validation
GLCM	Gray Level Co-occurrence Matrix
GLDM	Gray Level Dependence Matrix
GLRLM	Gray Level Run-Length Matrix
GLSZM	Gray Level Size Zone
KNN	K-nearest neighbors
NGTDM	Neighboring Gray Tone Difference Matrix
RF	Random forest
SD	Standard deviation

Introduction

Unilateral lymphadenopathy is a known finding following COVID-19 mRNA vaccine [1, 2]. It may be found incidentally on imaging examinations performed for different reasons such as routine screening or oncologic surveillance in mammography [3], breast magnetic resonance imaging (MRI) [4], or positron-emission tomography/computed tomography (PET/CT) [5].

The presence of ipsilateral fluorodeoxyglucose (FDG)-avid axillary lymph nodes after COVID-19 mRNA vaccination might challenge study interpretation, specifically in malignancies with a tendency to involve the axilla, of which breast cancer is the most common in women [6]. Discrimination between COVID-19 mRNA vaccine-associated FDG-avid lymph nodes and malignant lymph nodes using qualitative and quantitative variables may be impossible; therefore, to avoid potential conflicting findings it was recommended to schedule and plan scans wisely [7]. As FDG PET/CT cannot always be postponed, and must sometimes be conducted in proximity to the administration of the COVID-19 mRNA vaccine (e.g., in case of acute symptoms or urgent treatment planning), there is an unmet need to develop objective variables to identify COVID-19 mRNA vaccine-associated FDG-avid lymph nodes.

Radiomics and machine learning are emerging fields in medical image analysis designed for decision support of precision medicine. Radiomics is a relatively new technique for extracting quantitative variables that cannot be visually assessed in medical images [8, 9]. This technique uses intensity distribution (texture analysis) of pixel or voxel gray levels and pixel/voxel inter-connections within a region or volume of interest (e.g., tumor, lymph node) to extract these variables. In patients with cancer, first-order histogram variables (e.g., tumor shape, heterogeneity, uniformity) and second-order texture variables (e.g., Gray Level Co-occurrence Matrix [GLCM], Gray Level Dependence Matrix [GLDM]) can be used to characterize tumors [10–12] and have been correlated with tumor aggressiveness [13] and prognosis [14]. Machine learning

models study pre-input samples with known labels (known as training data) and identify patterns from which they learn a general rule that maps inputs to outputs [15]. To date, there are no published data on the use of PET/CT radiomics as a tool to differentiate FDG-avid metastatic axillary lymph nodes from FDG-avid reactive lymph nodes.

In this retrospective analysis, we used radiomics and machine learning tools to distinguish between FDG-avid metastatic axillary lymphadenopathy in breast cancer patients and FDG-avid reactive axillary lymph nodes in individuals who were vaccinated with the BNT162b2 (Comirnaty®) COVID-19 mRNA vaccine (Pfizer-BioNTech).

Materials and methods

Patients

FDG axillary lymph node uptake was analyzed in 2 patient populations:

1. *Patients with breast cancer:* Records of adult patients (> 18 years) with a diagnosis of breast cancer who underwent FDG PET/CT scans for follow-up or staging between 1 January 2019 and 30 November 2020 were retrieved. Then, a case-by-case search was performed using the picture archive and communication system (PACS; Carestream Vue PACS version 12.1.5.1) and the patients' medical records to obtain the ones showing avid FDG axillary lymph node uptake ipsilateral to the primary breast tumor and a positive lymph node histology showing breast malignancy. Information on lymph node histology was obtained from pathological records of post-surgery axillary lymph node dissections or from core needle biopsies of suspected axillary lymph nodes. Only records of patients with invasive breast carcinoma (i.e., infiltrating ductal carcinoma or infiltrating lobular carcinoma) were included. Records of breast cancer patients with no FDG axillary lymph node uptake, patients under 18 years, lesions not eligible for segmentation (due to a metal clip in the lymph node, post-surgery changes, uptake overlap among nodes, etc.), second primary tumors, unavailable medical records, and cases with an unknown lymph node pathology were excluded.

2. *Patients post-mRNA COVID-19 mRNA vaccine:* Consecutive FDG PET/CT scans were performed for any indication in adult patients (> 18 years) who received 1–2 injections of the BNT162b2 vaccine between 27 December 2020 and 31 January 2021 (December 2020 was the initiation date of a national COVID-19 vaccination rollout in the general population), and who showed positive FDG axillary lymph node uptake in the draining axillary lymph node on the vaccination side. Part of this cohort was recently described elsewhere [16]. Records of patients with breast

cancer, lymphoma, or a known malignancy involving axillary lymph nodes were excluded from the analysis. Records with low-quality PET/CT images (movement artifacts), missing medical information, or lesions that were ineligible for segmentation (e.g., due to very small lymph nodes, uptake overlap among nodes, metal artifacts) were also excluded.

Only contrast-enhanced CT scans were included in the analysis of both groups.

The institutional ethics committee approved the study (approval number 8069-21-SMC). The requirement for patient informed consent was waived.

FDG PET/CT acquisition

Most PET/CT examinations (88%) were performed according to our institute's clinical scanning protocols. Diagnostic CT examinations were performed on a 64-detector-row helical CT scanner (Philips Vereos, Philips Medical Systems). The field of view and pixel size of the PET images reconstructed for fusion were 57.6 cm and 4 mm, respectively, with a matrix size of 144×144 . The technical parameters used for CT imaging were as follows: pitch 0.83, gantry rotation speed 0.5 s/rot, 120 kVp, modulated tube current 40–300 mA, and specific breath-holding instructions. The patients received an intravenous injection of 5.18 MBq/kg after fasting for 6 h. About 60 min after tracer administration, CT images were obtained from the vertex to the mid-thigh or for the whole body. An emission PET scan followed in 3D acquisition mode for the same longitudinal coverage, 1.5 min per bed position. CT images were fused with the PET data to generate a map for attenuation correction, eventually generating reconstructed images for review on a computer workstation.

To increase the diversity of image samples in our cohort in order to ensure the prediction credibility of the machine learning models [17], 12% of the scans were performed using other scanners (n = number of scans): Discovery IQ (GE Healthcare) (n = 1), Ingenuity TF PET/CT (Philips Medical Systems) (n = 2), Gemini TF 16 (Philips Medical Systems) (n = 4), Guardian Body (C) (Philips Medical Systems) (n = 4), Biograph Vision 450 (Siemens Healthineers) (n = 1).

Image analysis

Image analysis was carried out using the PACS (Carestream Vue PACS version 12.1.5.1). All PET/CT scans were read by a board-certified radiologist currently undergoing a nuclear medicine residency with 3 years of experience in reading PET/CTs (M.E.).

Each FDG-positive axillary lymph node ipsilateral to the primary breast tumor or to the vaccine injection side

was segmented on the PET images and on the contrast-enhanced CT images using the PACS semi-automatic segmentation tool or a manual lesion tool, respectively (Fig. 1).

Positive axillary lymph node uptake was defined as having a ratio > 2 between the maximum standardized uptake value in the ipsilateral axillary nodes (for the tumor or vaccine side) and the contralateral reference sites. This method was previously used by Thomassen et al [18].

Feature extraction

Before features were extracted, all images were normalized by standardization (centering to $\mu = 0$, standard deviation [SD] = 1) to reduce the noise between scanners and to ensure data analysis on the same scale [17]. In total, 110 known radiomics features based on Image Biomarkers Standardization Initiative histogram analysis [19] were extracted from the PET and CT scans separately for each lymph node segment. Radiomics features were classified as first-order (18 features), Gray Level Co-occurrence Matrix (GLCM) (24 features), Gray Level Dependence Matrix (GLDM) (14 features), Gray Level Run-Length Matrix (GLRLM) (16 features), Gray Level Size Zone (GLSZM) (16 features), Neighboring Gray Tone Difference Matrix (NGTDM) (5 features), and shape (14 features).

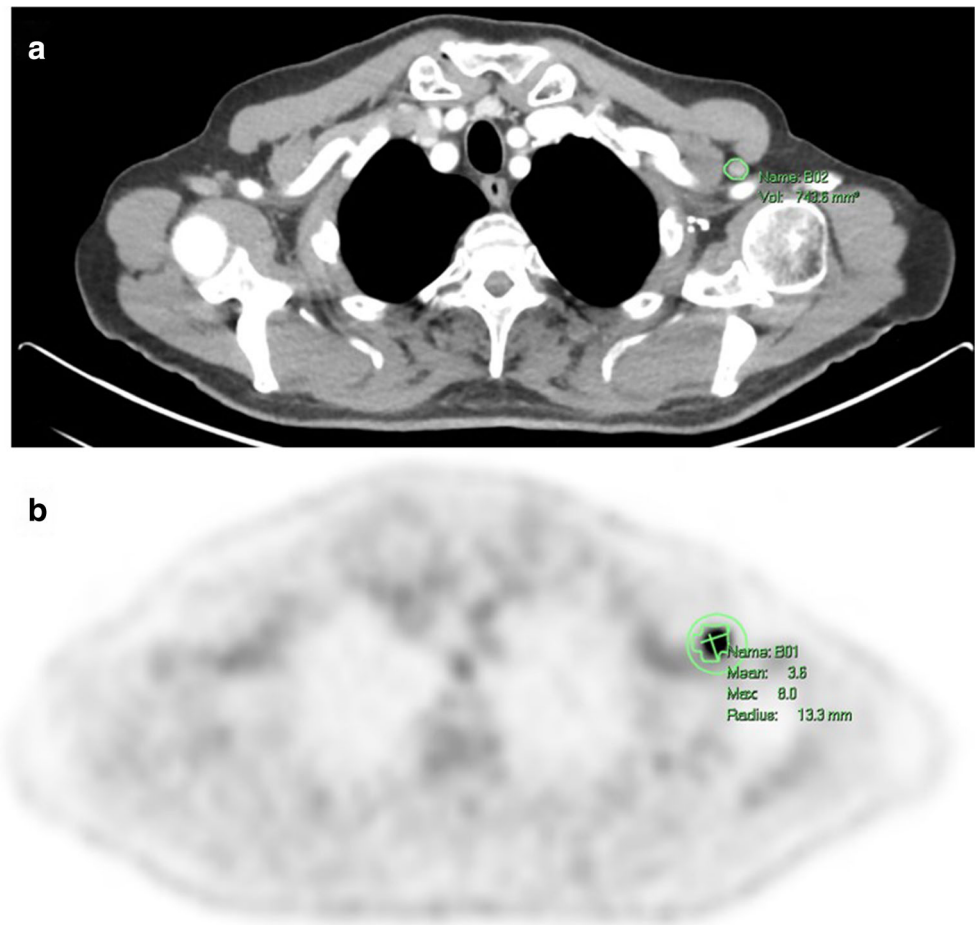
Data analysis and machine learning

To examine the metabolic process of the lesions and the effect of uptake values, the initial analysis focused on first-order features. This feature type produces a histogram analysis at pixel value level, for example, energy (associated with uptake score), entropy (the state of randomness in the segment, associated with the level of heterogeneity), and uniformity (indicating homogeneity).

Next, data analysis was performed using two supervised machine learning classification models: K-nearest neighbors (KNN) [20] and random forest (RF) [21]. For a deeper analysis, the radiomics features of 3 inputs were compared: CT, PET, and combined (add) PET/CT features as one input. For each input, seven radiomics feature groups were analyzed separately on the machine learning models. Additional standardization was performed before analyzing each input.

The model's performance was estimated using a 5-fold cross-validation which was done by splitting and randomizing the input data into training and testing (validation) sets comprising 132 and 33 lymph nodes, respectively. The 5-fold cross-validation was repeated ten times, with a calculation of mean and SD.

Fig. 1 A representative image of a 79-year-old male who had an FDG PET/CT for melanoma follow-up 3 days after receiving the second Pfizer-BioNTech COVID-19 mRNA vaccine in his left arm. Avid left axillary lymph node was segmented in **a** a contrast-enhanced CT and **b** a PET scan



Due to the small data size and to avoid overfitting, data augmentation was added to the training data set using left to right flipping and brightness (of 0.4) and contrast adjustments (of 2). Radiomics features were extracted from all augmented data.

Statistical analysis

The *t* test and chi-squared test were used for comparing continuous and categorical variables, respectively.

Two-tailed $p < 0.05$ was considered statistically significant. Data accuracy (the percentage of correct results), receiver operating characteristic (ROC) curve, the area under the curve (AUC), and confusion matrix were used to display machine learning mean result performance on the validation data set. Analysis and feature extraction were performed by the Python software (version 3.6), using the Pyradiomics [22], Scikit-learn 0.23.2 [23], and TensorFlow 2.3.0 [24] libraries.

Table 1 Demographic characteristics of the study population

Variable	All patients, <i>n</i> = 99	Post-COVID-19 mRNA vaccine*, <i>n</i> = 46	Breast cancer, <i>n</i> = 53	<i>p</i> value
Age (years)	61 ± 13 (30–86)	67 ± 9 (46–85)	57 ± 13 (30–86)	< 0.001‡
Females	77 (77%)	24 (52%)	53 (100%)	< 0.001†
Lymph node volume (cm ³)	95 ± 101 (7.5–575)	74 ± 88 (7.5–483)	115 ± 108 (13–575)	< 0.05‡

Categorical values are shown as number and percentage and continuous variables are shown as mean ± standard deviation (range)

*The post-vaccine group included patients with solid tumors: melanoma, gastro-intestinal, head and neck, hepatobiliary, genitourinary, lung, and sarcoma

‡ *p* value by the *t* test

† *p* value by the chi-squared test

Results

Patient demographics

The study flow chart is presented in Fig. 2 and patient demographics are shown in Table 1. The study population consisted of 99 patients (77.8% females) aged 61 ± 13 years (range, 30–86 years) with FDG PET/CT–positive axillary lymph nodes. On average, the breast cancer patient group was significantly younger than the post-COVID-19 mRNA vaccine group ($p < 0.001$). A total of 165 axillary lymph nodes were included in the analysis, 85 of them were pathology-proven breast cancer lymph nodes (median 1.6 nodes/patient, range 1–4) and 80 were post-COVID-19 mRNA vaccine axillary lymph nodes (median 1.7 nodes/patient, range 1–4). Average lymph node volume was significantly greater in the breast cancer group compared to the vaccine group ($p < 0.05$).

Radiomics analysis

Comparison of first-order radiomics features of the two groups showed statistically significant differences in all tested combined PET/CT features, in most of the tested PET features ($n = 15$), and in half of the CT features. All features are listed in Table 2. The distribution of the first-order PET features of the two groups is shown in Fig. 3.

Machine learning framework

Machine learning analysis of the 3 input data sets—CT, PET, and combined PET/CT—using the RF and KNN models, showed that the combined PET/CT input had the highest

Table 2 p value results of first-order feature analysis of CT, PET, and combined PET/CT in the study population

First-order features	PET/CT	CT	PET
10 percentile	0.002	0.31	0.002
90 percentile	< 0.001	0.06	< 0.001
Energy	0.003	0.01	0.02
Entropy	0.005	0.64	< 0.001
Inter quartile range	0.004	< 0.001	0.003
Kurtosis	< 0.001	0.02	0.06
Maximum	< 0.001	0.12	< 0.001
Mean absolute deviation	< 0.001	< 0.001	< 0.001
Mean	< 0.001	0.31	< 0.001
Median	< 0.001	0.66	< 0.001
Minimum	0.008	0.13	0.005
Range	< 0.001	0.35	< 0.001
Robust mean absolute deviation	Nan	< 0.001	Nan
Root mean squared	< 0.001	0.3	< 0.001
Skewness	< 0.001	< 0.001	0.77
Total energy	0.003	0.01	0.022
Uniformity	0.02	0.6	0.001
Variance	0.002	< 0.001	0.003

SD standard deviation, *Nan* not a number

AUC values followed by the CT and PET inputs (Table 3; Fig. 4).

The first-order, GLRLM, and GLDM feature groups had AUC values above 0.9. In the KNN model, these features showed test AUCs of 0.98, 0.96, and 0.95 and test accuracies of 96%, 91%, and 91%, respectively, for the combined PET/CT input. In the RF model, these features showed test

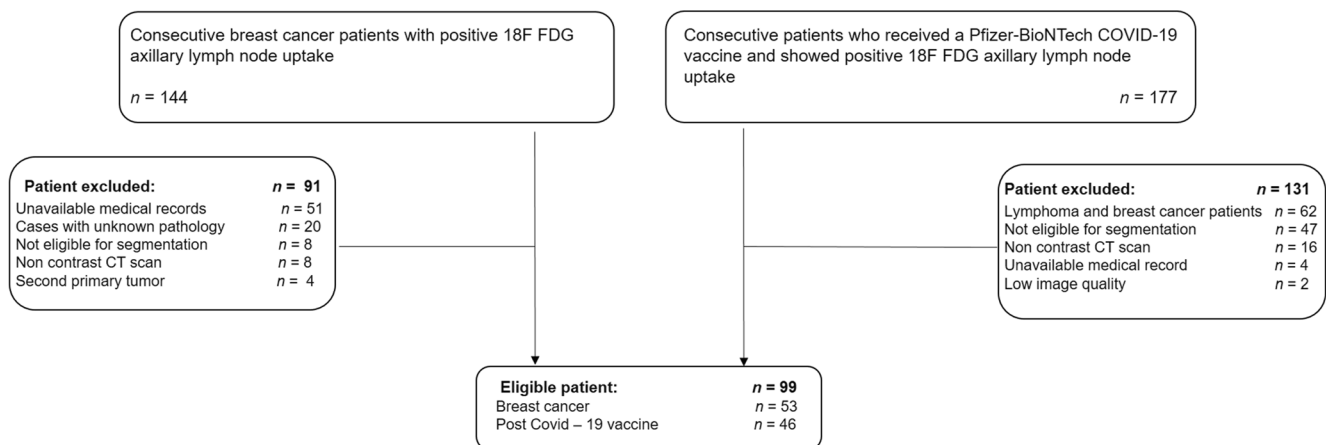


Fig. 2 Patient flow chart

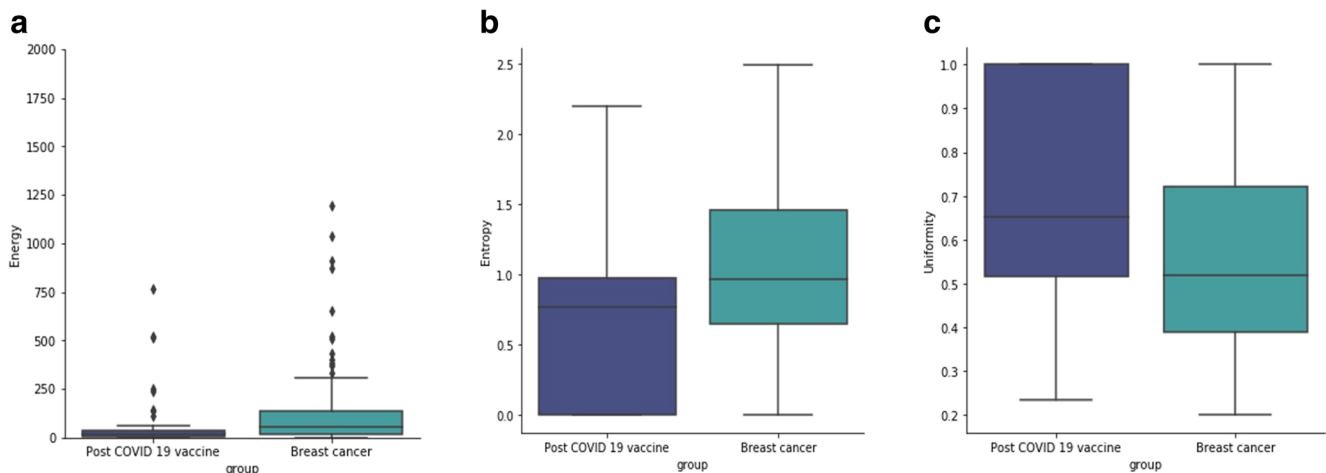


Fig. 3 Distribution of PET radiomics features. **a** Energy. **b** Entropy. **c** Uniformity

AUCs of 0.95, 0.93, and 0.94 and test accuracies of 88%, 84%, and 86%, respectively, for the combined PET/CT input.

Both CT and PET inputs showed the best results for first-order features. The RF model showed the best results for CT

inputs, with a test AUC of 0.96 and test accuracy of 90%. The KNN model showed the best result for PET inputs with a test AUC of 0.88 and test accuracy of 85%.

ROC curves for all feature groups of the combined PET/CT inputs are shown in Fig. 5.

Table 3 Summarized results (train and test accuracy and test AUC) of the machine learning random forest and k-nearest neighbor models for combined PET/CT, CT, and PET inputs

		Random forest			K-nearest neighbors		
		Train accuracy mean \pm SD	Test accuracy mean \pm SD	Test AUC mean \pm SD	Train accuracy mean \pm SD	Test accuracy mean \pm SD	Test AUC mean \pm SD
PET/CT	First-order	1.0 \pm 0.0	0.88 \pm 0.07	0.93 \pm 0.05	0.96 \pm 0.0	0.96 \pm 0.04	0.98 \pm 0.03
	GLCM	0.93 \pm 0.0	0.75 \pm 0.09	0.85 \pm 0.07	0.89 \pm 0.01	0.82 \pm 0.09	0.87 \pm 0.08
	GLRLM	1.0 \pm 0.0	0.84 \pm 0.09	0.95 \pm 0.05	0.96 \pm 0.0	0.91 \pm 0.07	0.95 \pm 0.06
	GLDM	1.0 \pm 0.0	0.86 \pm 0.06	0.92 \pm 0.06	0.95 \pm 0.0	0.91 \pm 0.05	0.96 \pm 0.05
	NGTDM	0.93 \pm 0.0	0.64 \pm 0.09	0.73 \pm 0.09	0.84 \pm 0.01	0.67 \pm 0.08	0.71 \pm 0.1
	GLSZM	1.0 \pm 0.0	0.77 \pm 0.09	0.85 \pm 0.07	0.92 \pm 0.0	0.81 \pm 0.09	0.86 \pm 0.06
	shape	1.0 \pm 0.0	0.76 \pm 0.07	0.82 \pm 0.09	0.94 \pm 0.0	0.78 \pm 0.08	0.83 \pm 0.09
CT	First-order	1.0 \pm 0.0	0.9 \pm 0.06	0.96 \pm 0.04	0.99 \pm 0.0	0.93 \pm 0.06	0.96 \pm 0.05
	GLCM	0.79 \pm 0.0	0.63 \pm 0.09	0.7 \pm 0.12	0.74 \pm 0.0	0.66 \pm 0.08	0.68 \pm 0.08
	GLRLM	1.0 \pm 0.0	0.79 \pm 0.1	0.87 \pm 0.09	0.96 \pm 0.0	0.81 \pm 0.11	0.84 \pm 0.1
	GLDM	1.0 \pm 0.0	0.76 \pm 0.08	0.84 \pm 0.08	0.96 \pm 0.0	0.79 \pm 0.09	0.82 \pm 0.09
	NGTDM	0.79 \pm 0.0	0.55 \pm 0.09	0.63 \pm 0.1	0.73 \pm 0.01	0.57 \pm 0.09	0.61 \pm 0.09
	GLSZM	0.94 \pm 0.0	0.62 \pm 0.1	0.68 \pm 0.08	0.89 \pm 0.01	0.64 \pm 0.09	0.67 \pm 0.1
	shape	1.0 \pm 0.0	0.78 \pm 0.09	0.85 \pm 0.1	0.97 \pm 0.0	0.86 \pm 0.08	0.87 \pm 0.1
PET	First-order	1.0 \pm 0.0	0.65 \pm 0.09	0.72 \pm 0.1	0.94 \pm 0.0	0.85 \pm 0.09	0.88 \pm 0.07
	GLCM	0.81 \pm 0.0	0.71 \pm 0.08	0.76 \pm 0.09	0.7 \pm 0.01	0.64 \pm 0.1	0.69 \pm 0.09
	GLRLM	0.81 \pm 0.0	0.67 \pm 0.08	0.73 \pm 0.1	0.74 \pm 0.02	0.63 \pm 0.09	0.71 \pm 0.08
	GLDM	0.8 \pm 0.0	0.7 \pm 0.07	0.76 \pm 0.07	0.73 \pm 0.02	0.67 \pm 0.08	0.74 \pm 0.08
	NGTDM	0.8 \pm 0.0	0.58 \pm 0.07	0.63 \pm 0.07	0.75 \pm 0.01	0.62 \pm 0.1	0.66 \pm 0.09
	GLSZM	0.79 \pm 0.0	0.69 \pm 0.07	0.75 \pm 0.08	0.71 \pm 0.02	0.65 \pm 0.1	0.71 \pm 0.09
	shape	0.68 \pm 0.01	0.55 \pm 0.09	0.59 \pm 0.1	0.71 \pm 0.02	0.56 \pm 0.09	0.59 \pm 0.09

GLCM Gray Level Co-occurrence Matrix, GLDM Gray Level Dependence Matrix, GLRLM Gray Level Run-Length Matrix, GLSZM Gray Level Size Zone Matrix, NGTDM Neighboring Gray Tone Difference Matrix, SD standard deviation

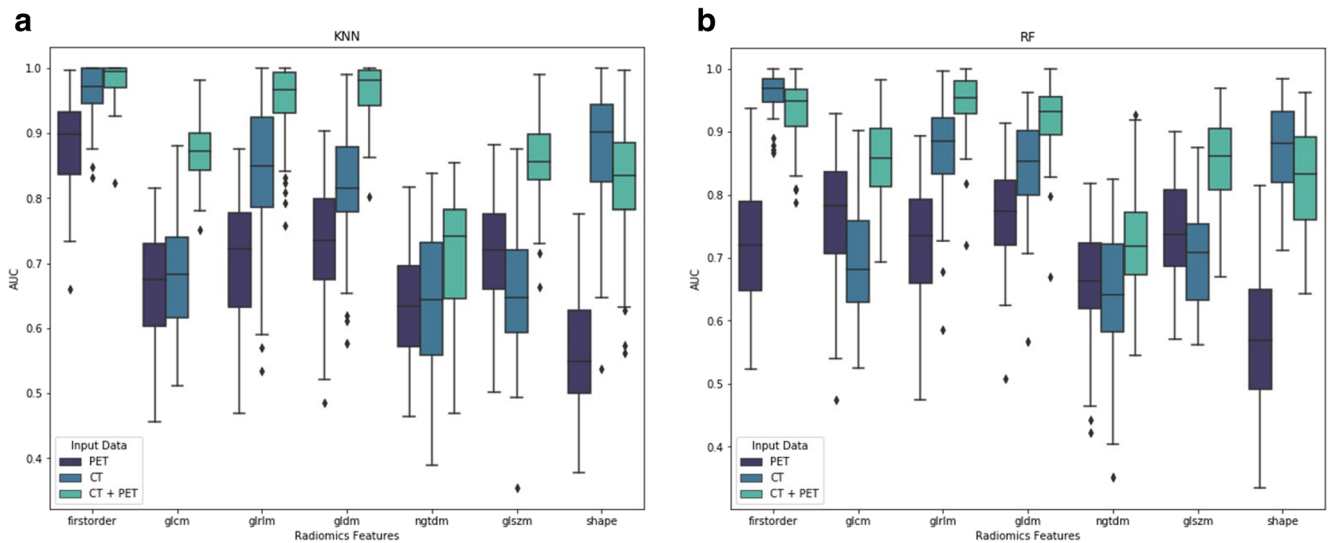


Fig. 4 Area under the curve (AUC) distribution (10 times of 5-fold) of PET, CT, and combined PET/CT radiomics features. **a** K-nearest neighbors (KNN) model. **b** Random forest (RF) model

Discussion

Our analysis demonstrates that FDG PET/CT radiomics features can distinguish between breast cancer and reactive COVID-19 mRNA vaccine lymphadenopathy. Since the initiation of the worldwide COVID-19 vaccination rollout, several studies have reported the incidence and intensity of FDG-avid axillary lymph nodes ipsilateral to the injection site and described the association between FDG avidity and variables such as age and immune status [16]. The incidence of ipsilateral FDG-avid lymph nodes is related to the number of vaccine doses administered, and has been reported to be 43–54% after the second vaccine dose [25–27] with persistent FDG uptake that can be seen beyond 6 weeks after the administration of the second vaccine dose [28].

It has been shown that a higher probability for positive FDG uptake in ipsilateral lymph nodes is correlated with longer elapsed time since the last vaccine dose and with the number of vaccine doses administered to the patient. According to Eifer et al, this correlation suggests that the metabolic activity reflects the activation of the immune system. In contrast, FDG uptake in the injection site reflects an inflammatory reaction [16].

In patients with several lesions suspected as malignant, a biopsy is usually performed on a single lesion, often on the one that is most accessible rather than on the most suspicious lesion, under the assumption that all additional lesions have similar characteristics and features to the sampled lesion. Radiomics may complement biopsies, as it can non-invasively characterize tumor heterogeneity in the whole tumor and potentially direct the biopsy needle to the most suspicious area. In addition, as radiomics analysis can be conducted on

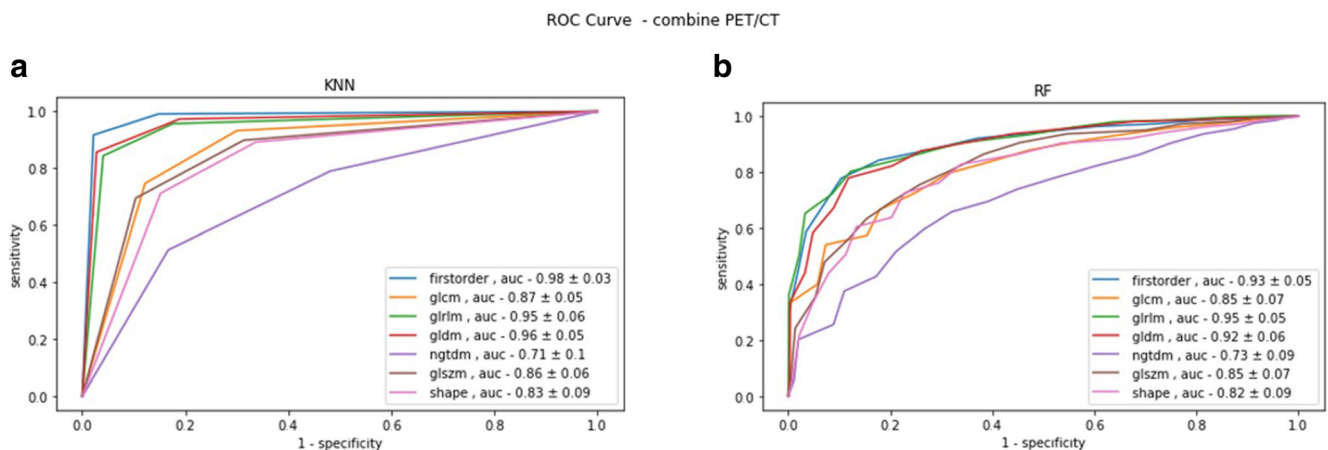
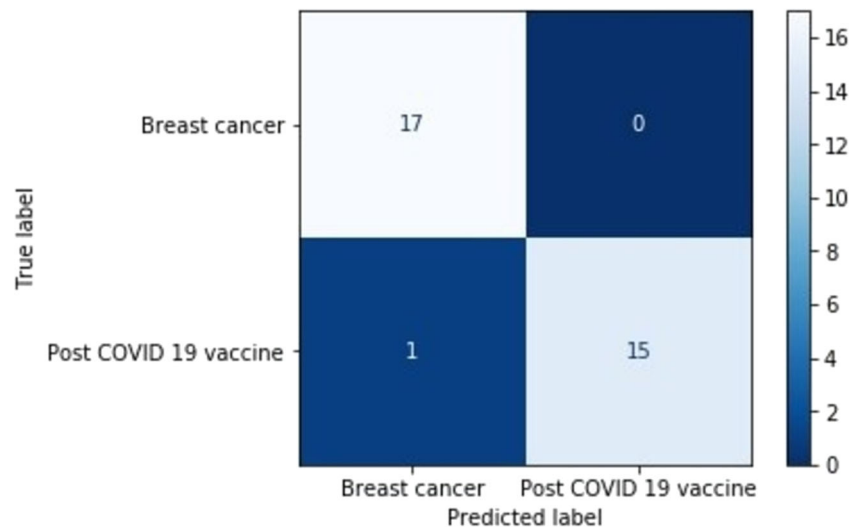


Fig. 5 Receiver operating curve (ROC) of the combined PET/CT radiomics features using machine learning models. **a** K-nearest neighbors (KNN) model. **b** Random forest (RF) model

Fig. 6 Confusion matrix for the k-nearest neighbors (KNN) model, first-order of combined input (PET/CT)



several metastases in the same patient, it is possible to compare variables among metastases. Not surprisingly, the use of radiomics with CT and MRI has become increasingly popular, and more recently it has been applied to PET [29].

Although most radiomics studies have characterized primary tumors, several studies have used it to characterize lymph nodes. Zheng et al [30] have shown that radiomics of FDG PET/CT studies in patients with breast cancer, with variables extracted from both the CT and PET portions, can distinguish between lymph nodes invaded by lymphoma and metastatic lymph nodes, with AUC, sensitivity, specificity, and accuracy of 0.95, 91.7%, 94.3%, and 92.7%, respectively.

To the best of our knowledge, this is the first study that uses radiomics to differentiate breast cancer metastatic lymph nodes from post-COVID-19 mRNA vaccine-associated lymph nodes. We have shown that first-order variables, specifically those reflecting tumor homogeneity, such as entropy and uniformity, are among the most statistically significant variables for distinguishing metastatic from post-COVID-19 vaccine-associated lymph nodes. Unfortunately, to date, no studies have examined lymph nodes histologically after COVID-19 mRNA vaccination in such a way that would have allowed conclusions to be drawn; however, Placke et al reported a lymph node dissection due to suspected malignancy in a patient who received a COVID-19 vaccine. Only marked follicular hyperplasia was found [31]. In this type of reaction, the lymph node follicles enlarge at the expense of other nodal structures and therefore, the lymph node becomes relatively more homogeneous. This observation is in line with Fan et al's findings that reactive lymph nodes are more homogeneous on an apparent diffusion coefficient distribution map compared to tumor metastatic lymph nodes [32]. In the present study, we demonstrated that the combination of PET and CT data improves test accuracy, as shown in the confusion matrix (Fig. 6), corroborating Zheng et al's findings, which demonstrated the added value of combining PET and CT radiomics [30].

This study has several limitations. First, the retrospective nature of the study has inherent biases. Second, the number of patients analyzed is relatively small and therefore, definite conclusions cannot be drawn. The small sample size also prevented us from performing deep learning analyses. However, despite the relatively small sample, the differences between the groups were statistically significant. Third, there was an age difference between the two groups that might have influenced the results, although in our opinion if there was an effect it is negligible. Last, several scans were performed on different PET/CT machines; however, we used a standardization method to overcome this obstacle.

In conclusion, this pilot study has shown that FDG PET/CT radiomics features can differentiate between FDG-avid metastatic axillary lymph nodes in patients with breast cancer and FDG-avid lymph nodes that are reactive to the COVID-19 mRNA vaccine. Further larger studies are needed to validate these results and to evaluate if this method can also be applied to differentiate benign lymphadenopathy from a malignant one in other conditions where the clinical assessment is not so helpful.

Funding The authors state that this work has not received any funding.

Declarations

Guarantor The scientific guarantor of this publication is Dr. Liran Domachevsky.

Conflict of interest The authors of this manuscript declare no relationships with any companies whose products or services may be related to the subject matter of the article.

Statistics and biometry One of the authors has significant statistical expertise.

Informed consent Written informed consent was waived by the Institutional Review Board.

Ethical approval Institutional Review Board approval was obtained.

Study subjects or cohorts overlap Some study subjects or cohorts have been previously reported in Eifer M, Tau N, Alhoubani Y, et al (2021) COVID-19 mRNA vaccination: age and immune status and its association with axillary lymph node PET/CT uptake. *J Nucl Med.* <https://doi.org/10.2967/jnumed.121.262194>

Methodology

- retrospective
- diagnostic or prognostic study
- performed at one institution

References

1. El Sahly HM, Baden LR, Essink B et al (2021) Efficacy of the mRNA-1273 SARS-CoV-2 vaccine at completion of blinded phase. *N Engl J Med* 385:1774–1785
2. Polack FP, Thomas SJ, Kitchin N et al (2020) Safety and efficacy of the BNT162b2 mRNA COVID-19 vaccine. *N Engl J Med* 383:2603–2615
3. Robinson KA, Maimone S, Gococo-Benore DA et al (2021) Incidence of axillary adenopathy in breast imaging after COVID-19 vaccination. *JAMA Oncol* 7:1395–1397
4. Edmonds CE, Zuckerman SP, Conant EF (2021) Management of unilateral axillary lymphadenopathy detected on breast MRI in the era of COVID-19 vaccination. *AJR Am J Roentgenol* 217:831–834
5. Orevi M, Chicheportiche A, Ben-Haim S (2021) Lessons learned from post-COVID-19 vaccination PET/CT studies. *J Nucl Med.* <https://doi.org/10.2967/jnumed.121.262348>
6. Bray F, Ferlay J, Soerjomataram I et al (2018) Global cancer statistics 2018: GLOBOCAN estimates of incidence and mortality worldwide for 36 cancers in 185 countries. *CA Cancer J Clin* 68:394–424
7. Becker AS, Perez-Johnston R, Chikarmane SA et al (2021) Multidisciplinary recommendations regarding post-vaccine adenopathy and radiologic imaging: radiology scientific expert panel. *Radiology* 300:E323–E327
8. Gillies RJ, Kinahan PE, Hricak H (2016) Radiomics: images are more than pictures, they are data. *Radiology* 278:563–577
9. Mayerhoefer ME, Materka A, Langs G et al (2020) Introduction to radiomics. *J Nucl Med* 61:488–495
10. Feng Q, Hu Q, Liu Y, Yang T, Yin Z (2020) Diagnosis of triple negative breast cancer based on radiomics signatures extracted from preoperative contrast-enhanced chest computed tomography. *BMC Cancer* 20:579
11. Zhu S, Xu H, Shen C et al (2021) Differential diagnostic ability of 18F-FDG PET/CT radiomics features between renal cell carcinoma and renal lymphoma. *Q J Nucl Med Mol Imaging* 65:72–78
12. Ou X, Wang J, Zhou R et al (2019) Ability of 18F-FDG PET/CT radiomic features to distinguish breast carcinoma from breast lymphoma. *Contrast Media Mol Imaging* 2019:4507694
13. Sala E, Mema E, Himoto Y et al (2017) Unravelling tumour heterogeneity using next-generation imaging: radiomics, radiogenomics, and habitat imaging. *Clin Radiol* 72:3–10
14. Cai D, Duan X, Wang W et al (2021) A metabolism-related radiomics signature for predicting the prognosis of colorectal cancer. *Front Mol Biosci* 7:613918
15. Choy G, Khalilzadeh O, Michalski M et al (2018) Current applications and future impact of machine learning in radiology. *Radiology* 288:318–328
16. Eifer M, Tau N, Alhoubani Y et al (2021) COVID-19 mRNA vaccination: age and immune status and its association with axillary lymph node PET/CT uptake. *J Nucl Med.* <https://doi.org/10.2967/jnumed.121.262194>
17. Chatterjee A, Vallieres M, Dohan A et al (2019) Creating robust predictive radiomic models for data from independent institutions using normalization. *IEEE Trans Radiat Plasma Med Sci* 3:210–215
18. Thomassen A, Lerberg Nielsen A, Gerke O, Johansen A, Petersen H (2011) Duration of 18F-FDG avidity in lymph nodes after pandemic H1N1v and seasonal influenza vaccination. *Eur J Nucl Med Mol Imaging* 38:894–898
19. Zwanenburg A, Leger S, Vallieres M, Lock S (2016) Image biomarker standardization initiative - feature definitions. *arXiv:1612.07003*
20. Goldberger J, Roweis S, Hinton GE, Salakhutdinov RR (2005) Neighbourhood components analysis. In: Saul LK, Weiss Y, Bottou L, eds. *Advances in neural information processing systems* Vol 17. 2005:513–520.
21. Breiman L (2001) Random forests. *Mach Learn* 45:5–32
22. van Griethuysen JJM, Fedorov A, Parmar C et al (2017) Computational radiomics system to decode the radiographic phenotype. *Cancer Res* 77:e104–e107
23. Pedregosa F, Varoquaux G, Gramfort A et al (2011) (2012) Scikit-learn: machine learning in Python. *J Mach Learn Res* 12:2825–2830
24. Abadi M, Agarwal A, Barham P, et al (2016) TensorFlow: large-scale machine learning on heterogeneous distributed systems. *arXiv:1603.04467*
25. Cohen D, Krauthammer SH, Wolf I, Even-Sapir E (2021) Hypermetabolic lymphadenopathy following administration of BNT162b2 mRNA COVID-19 vaccine: incidence assessed by [18F]FDG PET-CT and relevance to study interpretation. *Eur J Nucl Med Mol Imaging* 48:1854–1863
26. Skawran S, Gennari AG, Dittli M et al (2021) [18F] FDG uptake of axillary lymph nodes after COVID-19 vaccination in oncological PET/CT: frequency, intensity, and potential clinical impact. *Eur Radiol.* <https://doi.org/10.1007/s00330-021-08122-2>
27. Bernstine H, Priss M, Anati T et al (2021) Axillary lymph nodes hypermetabolism after BNT162b2 mRNA COVID-19 vaccination in cancer patients undergoing 18F-FDG PET/CT: a cohort study. *Clin Nucl Med* 46:396–401
28. Eshet Y, Tau N, Alhoubani Y, Kanana N, Domachevsky L, Eifer M (2021) Prevalence of increased FDG PET/CT axillary lymph node uptake beyond 6 weeks after mRNA COVID-19 vaccination. *Radiology* 300:E345–E347
29. Piñero-Fiel M, Moscoso A, Pubul V, Ruibal A, Silva-Rodríguez J, Aguiar P (2021) A systematic review of PET textural analysis and radiomics in cancer. *Diagnostics (Basel)* 11. <https://doi.org/10.3390/diagnostics11020380>
30. Zheng B, Wu J, Zhao Z, Ou X, Cao P, Ma X (2020) Distinguishing lymphomatous and cancerous lymph nodes in 18F-fluorodeoxyglucose positron emission tomography/computed tomography by radiomics analysis. *Contrast Media Mol Imaging* 2020:1–15
31. Placke J-M, Reis H, Hadaschik E et al (2021) Coronavirus disease 2019 vaccine mimics lymph node metastases in patients undergoing skin cancer follow-up: a monocentre study. *Eur J Cancer* 154:167–174
32. Zhang F, Zhu L, Huang X, Niu G, Chen X (2013) Differentiation of reactive and tumor metastatic lymph nodes with diffusion-weighted and SPIO-enhanced MRI. *Mol Imaging Biol* 15:40–47

Publisher's note Springer Nature remains neutral with regard to jurisdictional claims in published maps and institutional affiliations.